Proceedings of IMECE04
2004 ASME International Mechanical Engineering Congress and Exposition
November 13-20, 2004, Anaheim, California USA

IMECE2004-62378

QUASI-STEADY ANALYSIS OF A MAGNETORHEOLOGICAL DASHPOT DAMPER

Young-Tai Choi and Norman M. Wereley
Smart Structures Laboratory, Alfred Gessow Rotorcraft Center
Department of Aerospace Engineering, University of Maryland
College Park, Maryland 20742, USA

ABSTRACT

This paper addresses quasi-steady analysis of a magnetorheological (MR) dashpot damper. MR dashpot dampers show mixed fluid mode of flow and shear flows since a dashpot inside dampers works as a piston and a moving wall simultaneously. In this study, quasi-steady analysis of MR dashpot dampers has developed based on the utilization of the Bingham-plastic constitutive model to assess performance metrics such as damping capacity. For the mixed mode MR damper that is the sums of flow and shear flows, fluid velocity profile, shear stress profile, and damping coefficient are theoretically derived. In addition, the preyield thickness equation to characterize the relationship between the Bingham number and the preyield thickness is constructed. Through computer simulation, damping characteristics of the mixed mode MR dashpot damper are evaluated and compared with flow mode case.

INTRODUCTION

The inherent characteristics of MR (magnetorheological) fluids such as continuously controllable yield stress and fast response have prompted many researchers to develop novel dampers so as to reduce and isolate vibration and shock motion of devices.

Most of dampers have designed and manufactured based on three working fluid modes of damper operation: shear mode [1-3], flow mode [4-6], and squeeze mode [7-9]. The shear mode occurs when one of two magnetic poles moves linearly or rotationally relative to the other. In the shear mode, the fluid is directly sheared by relative motion of these surfaces. The flow mode is characterized by pressurized flow between two magnetic poles that form the opposite walls of a rectangular or annular duct. The squeeze mode occurs when the magnetic poles move toward each other, squeezing out the fluid. However, the shear mode dampers require large magnetic pole surface area contacted with the fluid in order to achieve high damper force, and the squeeze mode dampers can only work in the very small vibration situation. The flow mode is most advantageous for high force high stroke applications.

As an expansion of flow mode dampers, mixed mode MR dashpot dampers will be addressed in this study. MR dashpot dampers show mixed fluid mode of flow and shear flows since a dashpot inside dampers works as a piston and a moving wall simultaneously. Based on the utilization of the Bingham-plastic constitutive model, quasi-steady analysis of MR dashpot dampers has developed in order to assess performance metrics such as damping capacity. For the mixed mode MR damper, fluid velocity profile, shear stress profile, and damping coefficient are theoretically derived. In addition, the preyield thickness equation to characterize the relationship between Bingham number as a nondimensional input and the preyield thickness is constructed. Through computer simulation, damping characteristics of the mixed mode MR dashpot damper are evaluated and compared with flow mode case.

MR DASHPOT DAMPER

MR dashpot dampers have the mixed mode of working fluid operation such as flow (Poissieulle flow) and shear modes through the valve inside MR dampers. A schematic diagram of fluid velocity profile in the valve inside the MR dashpot damper is shown in Figure 1. As mentioned earlier, the dashpot works as a piston and a moving wall simultaneously.

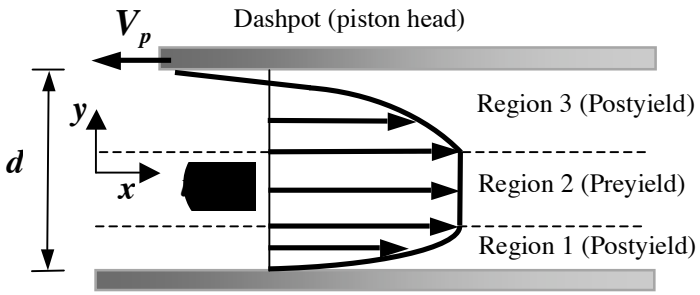

Figure 1. Schematic diagram of fluid velocity profile in the valve inside MR dashpot damper.

The other magnetic pole or wall configured by the outer cylinder of the damper is stationary. Note that the dashpot motion is reverse to the direction of the fluid velocity in the valve. This is because the pressure at the left side of the valve is higher to the pressure at the right side in the situation when the dashpot is moving to the left direction. Thus, the fluid pressured by the dashpot is passing from the left to right side of the valve.

THEORETICAL MODELING

The damper force F of MR dashpot damper can be given by

$$F = A_p \Delta P + A_s \tau_w \tag{1}$$

Here, A_p is the effective piston head area and ΔP is the pressure drop between both end sides of the MR valve. $A_s = bL$ is the side surface area of the piston head, b is the width of the valve, L is the active length of the valve, and τ_w is the resistant shear stress at the side surface of the piston head. The pressure drop at quasi-steady state can be obtained from force equilibrium in the annular duct as follows [10]:

$$\Delta P = -\left(\frac{d\tau}{dr} + \frac{\tau}{r} \right) L \tag{2}$$

Here, τ is the shear stress and r is the radial coordinate. Note that fluid acceleration term is neglected at Eq.(2). For high velocity flow or high frequency oscillatory flow, the fluid inertia term must be incorporated [10]. Approximating the 1D axisymmetric annular duct geometry of the valve by a rectangular duct, Eq.(2) simplifies to

$$\Delta P = -\frac{d\tau}{dy} L \tag{3}$$

Here, y is the coordinate originated from the center of the valve toward the wall of the valve.

Integrating Eq.(3) yields the shear stress profile in the valve

$$\tau = -\frac{\Delta P}{L} y + \alpha_\tau \tag{4}$$

Here, α_τ is the integration constant. The boundary conditions are

$$\tau\left(-y_{pi}\right) = \tau_y \quad \text{and} \quad \tau\left(y_{po}\right) = -\tau_y \tag{5}$$

which leads to $\alpha_\tau = 0$. Thus

$$\tau = -\frac{\Delta P}{L} y \tag{6}$$

From Eq.(6), the resistant shear stress at the side surface of the piston head is determined as follows:

$$\tau_w = \frac{\Delta P d}{2L} \tag{7}$$

Here, d is the gap in the valve. Substituting Eq.(7) into Eq.(1) yields the damping force of the MR dashpot damper

$$F = \left(A_p + \frac{A_d}{2} \right) \Delta P \tag{8}$$

Here, $A_d = bd$ is the cross-sectional area of the valve.

The constitutive equation for MR fluid for Bingham model for one-dimensional flow is well known

$$\tau = \tau_y \operatorname{sgn}(u) + \mu \left(\frac{du}{dy} \right) \tag{9}$$

Here, u is the fluid velocity, τ_y is the yield shear stress, and μ is the fluid viscosity.

Substituting Eq.(9) into Eq.(3) yields the relation

$$\left(\frac{d^2 u}{dy^2} \right) = -\frac{\Delta P}{\mu L} \tag{10}$$

Fluid Velocity Profile

Integrating Eq.(10) yields the fluid velocity gradient

$$u'(y) = \left(\frac{\alpha}{\mu} - \frac{\Delta P}{\mu L} y \right) \tag{11}$$

Here, α is the integration constant. Again, integrating the velocity gradient yields the fluid velocity profiles:

$$u(y) = \left(\frac{\alpha}{\mu} y - \frac{\Delta P}{\mu L} \frac{y^2}{2} \right) + \beta \tag{12}$$

Here, β is the integration constant. The fluid velocity u at mixed mode such as flow and shear flows is determined by boundary conditions and compatibility conditions. First, the boundary conditions are

$$u_1\left(-\frac{d}{2} \right) = 0 \quad \text{and} \quad u_3\left(\frac{d}{2} \right) = -V_p \tag{13}$$

Here, u_i implies the fluid velocity in the ith region and V_p is the dashpot velocity. The fluid velocity compatibility conditions are

$$u_1(-y_{pi}) = u_3(y_{po}) \tag{14}$$

Here, y_{pi} is the inner location of the preyield region and y_{po} is the outer location of the preyield region. Velocity gradient compatibility conditions must also be satisfied. Note that the plug or preyield region moves at constant velocity, since it is essentially a rigid, so that the velocity gradient across the plug must be zero. The velocity gradient compatibility conditions are

$$u_1'\left(-y_{pi}\right) = u_3'\left(y_{po}\right) = 0 \tag{15}$$

Note that, for flow mode analysis, the velocity symmetry condition must hold. Thus the plug is symmetric about the center of the valve. However, in the case of mixed mode such as flow and shear flows, the velocity symmetry does not hold. Thus the center of the plug is dependent on the piston velocity.

Region 1 (Postyield): $-\frac{d}{2} \le y \le -y_{pi}$ Two boundary conditions for region 1 are used to obtain the fluid velocity in the valve. First, the velocity gradient at the inner location of the preyield region given by Eq.(11) must be zero, to ensure compatibility of the shear rate. Hence

$$u_1'\left(-y_{pi}\right) = 0 = \left(\frac{\alpha_1}{\mu} + \frac{\Delta P}{\mu L} y_{pi}\right) \tag{16}$$

which yields an expression for the integration constant α_1, as below

$$\alpha_1 = -\frac{\Delta P}{L} y_{pi} \tag{17}$$

Applying no-slip condition at the bottom of the valve given by Eq.(13) into Eq.(12) yields the integration constant β_1, as below

$$\beta_1 = \left(\frac{\Delta P}{\mu L}\right)\left(\frac{d^2}{8} - \frac{y_{pi} d}{2}\right) \tag{18}$$

Substituting the integration constants yields the velocity profile for region 1:

$$u_1(y) = -\left(\frac{\Delta P}{2\mu L}\right)\left[\left(y + y_{pi}\right)^2 - \left(\frac{d}{2} - y_{pi}\right)^2\right] \tag{19}$$

Region 3 (Postyield): $y_{po} \le y \le \frac{d}{2}$ First, applying velocity gradient compatibility condition given by Eq.(15) into Eq. (11) yields the integration constant

$$u_3'\left(y_{po}\right) = 0 = \left(\frac{\alpha_3}{\mu} - \frac{\Delta P}{\mu L} y_{po}\right) \tag{20}$$

which yields an expression for the integration constant α_3, as below:

$$\alpha_3 = \frac{\Delta P}{L} y_{po} \tag{21}$$

From Eq.(12) with the boundary condition given by Eq.(13),

$$\begin{aligned} u_3\left(\frac{d}{2}\right) &= -V_p \\ &= \left(\frac{\alpha}{\mu}\frac{d}{2} - \frac{\Delta P}{\mu L}\frac{d^2}{8}\right) + \beta \end{aligned} \tag{22}$$

Finally, the fluid velocity profile for region 3 is obtained

$$u_3(y) = -\left(\frac{\Delta P}{2\mu L}\right)\left[\left(y - y_{po}\right)^2 - \left(\frac{d}{2} - y_{po}\right)^2\right] + V_p \tag{23}$$

Region 2 (Preyield): $-y_{pi} \le y \le y_{po}$ Because the velocity gradient must be zero across the preyield or plug region, the fluid velocity must be constant across the plug region as well. Thus using Eq.(14) yields the fluid velocity profile in region 2

$$\begin{aligned} u_2(y) &= \left(\frac{\Delta P}{2\mu L}\right)\left(\frac{d}{2} - y_{pi}\right)^2 \\ &= \left(\frac{\Delta P}{2\mu L}\right)\left(\frac{d}{2} - y_{po}\right)^2 + V_p \end{aligned} \tag{24}$$

Preyield Thickness

The preyield or plug thickness and its location in the valve can be determined using the shear stress boundary conditions. From Eqs.(5) and (6), the preyield thickness δ can be expressed as below:

$$\delta = y_{pi} + y_{po} = \frac{2L\tau_y}{\Delta P} \tag{25}$$

With Eqs.(24) and (25), solving for the location of the preyield thickness leads to

$$y_{pi} = \frac{1}{2}\left(\delta + y_c\right) \quad \text{and} \quad y_{po} = \frac{1}{2}\left(\delta - y_c\right) \tag{26}$$

where y_c is the center of the preyield thickness and expressed as

$$y_c = \frac{2\mu L V_p}{\Delta P\left(d - \delta\right)} \tag{27}$$

Note that, in this study, the origin of the y coordinate is the center of the valve. Introducing Bingham number Bi defined as below

$$Bi = \frac{\tau_y d}{\mu V_d} = \frac{\tau_y d}{\mu\left(\overline{A} - \frac{1}{2}\right)V_p} \tag{28}$$

where, V_d is the average fluid velocity in the valve and $\overline{A} = \left(\frac{A_p}{A_d}\right)$. the center of the preyield thickness in Eq.(27) can be written as

$$y_c = \frac{\overline{\delta}}{\left(\overline{A} - \frac{1}{2}\right)Bi\left(1-\overline{\delta}\right)} \tag{29}$$

where the nondimensional preyield thickness $\overline{\delta}$

$$\overline{\delta} = \frac{\delta}{d} \tag{30}$$

Preyield Thickness Equation

If the preyield thickness is determined, the damper force F of the dashpot damper can be easily obtained from Eqs.(8) and (25). The preyield thickness is obtained by solving preyield thickness equation which can be derived from equating flow rate Q_p displaced by piston to the flow rate through the valve. The flow rate Q_d through the valve is obtained by integration of the velocity profiles in each region:

$$\begin{aligned} Q_d &= b\int_{-\frac{d}{2}}^{-y_{pi}} u_1 dy + b\int_{-ypi}^{y_{po}} u_2 dy + b\int_{-ypo}^{\frac{d}{2}} u_3 dy \\ &= Q_p = \left(A_p - \frac{A_d}{2}\right)V_p \end{aligned} \tag{31}$$

With nondimensional variables such as nondimensional preyield thickness and Bingham number, rearranging Eq.(31) yields the preyield thickness equation for mixed mode analysis as below:

$$\frac{6\overline{A}\overline{\delta} + \sqrt{\left(6\overline{A}\overline{\delta}\right)^2 - 6\left(1+\frac{\overline{\delta}}{2}\right)\overline{\delta}^3}}{2\left(\overline{A}-\frac{1}{2}\right)\left(1-\overline{\delta}\right)^2\left(1+\frac{\overline{\delta}}{2}\right)} - Bi = 0 \tag{32}$$

Using binomial series [12], Eq.(32) simplifies to

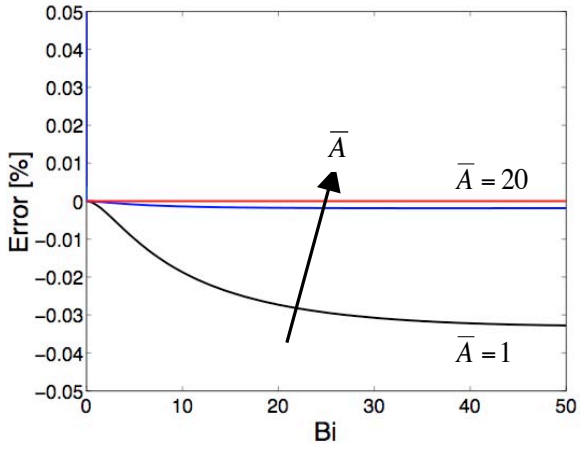

Figure 2. Errors of nondimensional preyield thickness between Eq.(32) and Eq.(33) versus Bingham number.

$$\frac{\overline{A}}{\left(\overline{A}-\frac{1}{2}\right)}\frac{6\overline{\delta}}{\left(1-\overline{\delta}\right)^2\left(1+\frac{\overline{\delta}}{2}\right)}\left[1-\left(\frac{\overline{\delta}}{24\overline{A}^2}\right)\left(1+\frac{\overline{\delta}}{2}\right)\right] - Bi = 0 \tag{33}$$

Errors of nondimensional preyield thickness between Eq.(32) and Eq.(33) are presented in Figure 2. As observed in Figure 2, $\overline{A}$ increases, the error decreases. The maximum error of simplified nondimensional preyield thickness in Eq.(33) is less than 0.04%. In this study, Eq.(33) will be used as the preyield thickness equation for the mixed mode MR dashpot damper.

On the other hand, note that, for flow mode analysis, the preyield thickness equation is given by [11,13]

$$\frac{6\overline{\delta}}{\left(1-\overline{\delta}\right)^2\left(1+\frac{\overline{\delta}}{2}\right)} - Bi = 0 \tag{34}$$

If $\overline{A} \to \infty$, the preyield thickness equation for mixed mode analysis given by Eq.(33) is exactly equal to that for flow mode analysis given by Eq.(34).

Given the piston velocity, V_p, the Bingham number, Bi is calculated, and nondimensional preyield thickness, $\overline{\delta}$, can be determined as the root of the nonlinear equation in Eq.(33) in its domain $0 < \overline{\delta} < 1$.

EQUIVALENT DAMPING

The damper force in Eq.(8) can be rewritten using Eq.(25)

$$F = \left(A_p + \frac{A_d}{2}\right)\frac{2\tau_y L}{\overline{\delta} d} \tag{35}$$

Using Eq.(28) and Eq.(33), the damper force of the mixed mode MR damper can be expressed as a function of the velocity as below:

$$F = C_{eq} V_p \tag{36}$$

where

$$C_{eq} = \frac{A_p\left(A_p + \frac{A_d}{2}\right)12\mu L}{bd^3}\left(\frac{1-\left(\frac{\bar{\delta}}{24\bar{A}^2}\right)\left(1+\frac{\bar{\delta}}{2}\right)}{\left(1-\bar{\delta}\right)^2\left(1+\frac{\bar{\delta}}{2}\right)}\right) \tag{37}$$

The damper force in the absence of field is $F_0 = C_0 V_p$, which implies that $\bar{\delta} = 0$, so that where

$$C_0 = \frac{A_p\left(A_p + \frac{A_d}{2}\right)12\mu L}{bd^3} \tag{38}$$

This leads to an expression for the damping coefficient, or the ratio of the field dependent damping C_{eq} to the damping in the absence of field, C_0, as below

$$\frac{C_{eq}}{C_0} = \left(\frac{1-\left(\frac{\bar{\delta}}{24\bar{A}^2}\right)\left(1+\frac{\bar{\delta}}{2}\right)}{\left(1-\bar{\delta}\right)^2\left(1+\frac{\bar{\delta}}{2}\right)}\right) \tag{39}$$

The above expression is a nondimensional representation of the damping capacity of the MR damper. Note that, for the flow mode analysis, the damping coefficient $\left(C_{eq}/C_0\right)_f$ is given by [11,13]

$$\left(\frac{C_{eq}}{C_0}\right)_f = \frac{1}{\left(1-\bar{\delta}\right)^2\left(1+\frac{\bar{\delta}}{2}\right)} \tag{40}$$

It is an interesting thing to check how much the mixed mode MR damper will show bigger damping coefficient than flow mode MR damper.

$$\Delta\left(\frac{C_{eq}}{C_0}\right) = \frac{\left(\frac{C_{eq}}{C_0}\right) - \left(\frac{C_{eq}}{C_0}\right)_f}{\left(\frac{C_{eq}}{C_0}\right)_f} = -\left(\frac{\bar{\delta}}{24\bar{A}^2}\right)\left(1+\frac{\bar{\delta}}{2}\right) \tag{41}$$

Here, $\Delta\left(C_{eq}/C_0\right)$ is the increment from the flow mode damping coefficient to the mixed mode damping coefficient. Since $0 \le \bar{\delta} \le 1$,

$$-\frac{1}{16\bar{A}^2} \le \Delta\left(\frac{C_{eq}}{C_0}\right) \le 0 \tag{42}$$

Thus, Eq.(42) implies that the mixed mode damping coefficient is equal or less than the flow mode damping coefficient. In addition, since $\bar{A} >> 1$ in general MR damper geometry and damping coefficient increase is proportional to $1/\bar{A}^2$, the difference between the mixed mode and flow mode damping coefficients is almost nothing in most of practical damper applications. Note that, absolute values of the equivalent damping C_{eq} or damping in the absence of field C_0 are not smaller than the flow mode case.

ANALYSIS RESULTS

The first performance diagram of the mixed mode MR dashpot damper is the damping coefficient $\left(C_{eq}/C_0\right)$, versus the Bingham number Bi. The damping coefficient linearly increases with respect to the Bingham number. As $\bar{A}$ increases, the damping coefficient for the mixed mode analysis is close to the flow mode result.

Figure 4 presents the nondimensional preyield thickness versus the Bingham number. As the Bingham number increases, the nondimensional preyield thickness increases like one-side sigmoid shape. This implies that the ratio of the yield shear stress over the viscous shear stress increases, or the yield stress becomes larger than the viscous shear stress, the extent of preyield region in the valve will increase. In addition, it demands for very large Bingham numbers so that the nondimensional plug thickness will approach unity. $\bar{\delta} = 1$ physically implies that the preyield region will completely fill

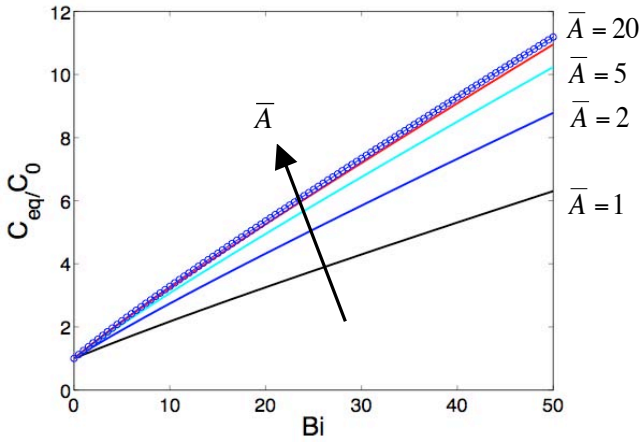

Figure 3. Damping coefficient versus Bingham number. The lines stand for the mixed mode results and the circle stands for the flow mode result.

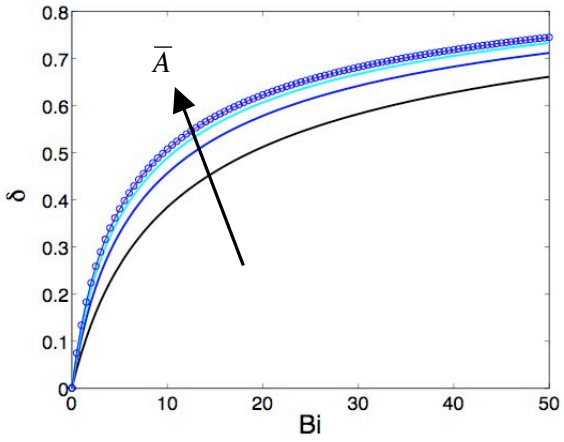

Figure 4. Nondimensional preyield thickness versus Bingham number. The lines stand for the mixed mode results and the circle stands for the flow mode result.

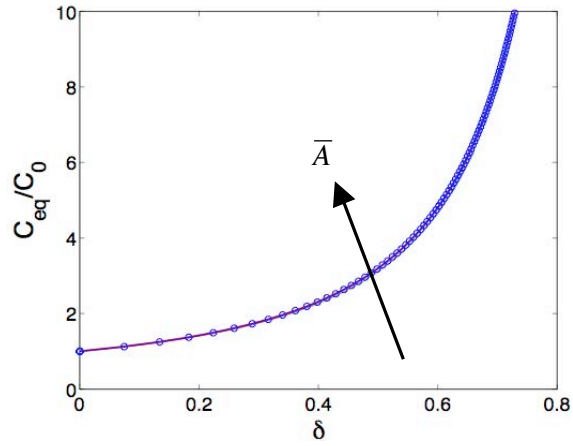

Figure 5. Damping coefficient versus nondimensional preyield thickness. The lines stand for the mixed mode results and the circle stands for the flow mode result.

the valve. On the other hand, as $\overline{A}$ increases, the nondimensional preyield thickness for the mixed mode analysis is also close to the flow mode result.

Figure 5 presents the damping coefficient versus the nondimensional preyield thickness as represented by Eq.(39). As the nondimensional preyield thickness increases, the damping coefficient dramatically increases. On the other hand, the damping coefficient versus the nondimensional preyield thickness plot for the mixed mode analysis is not much affected, as explained in Eq.(42).

CONCLUSIONS

Quasi-steady analysis for mixed mode MR dashpot dampers was addressed in this study. MR dashpot dampers show mixed fluid mode of flow and shear flows since a dashpot inside dampers works as a piston and a moving wall simultaneously. Based on the utilization of the Bingham-plastic constitutive model, quasi-steady analysis of MR dashpot dampers conducted in order to assess performance metrics such as damping capacity. For the mixed mode MR damper, fluid velocity profile, shear stress profile, and damping coefficient were theoretically derived. In the case of mixed mode such as flow and shear flows, the fluid velocity symmetry in the valve does not hold and the center of the plug or preyield region is dependent on the piston velocity. In addition, the preyield thickness equation to characterize the relationship between Bingham number as a nondimensional input and the preyield thickness was constructed and the exact preyield thickness equation can be successfully replaced by the approximation derived through binomial within the maximum error of 0.04%. Through computer simulation, damping characteristics of the mixed mode MR dashpot damper are evaluated and compared with flow mode case. The damping coefficient for the mixed mode analysis is equal or less than that for the flow mode analysis. In practical situation where $\overline{A}$ is greater than 5 or Bi is in small number, the mixed mode results is almost similar to the flow mode result.

REFERENCES

[1] Choi, S.B., Choi, Y.T., Cheong, C.C. and Jeon, Y.S. (1999) "Performance Evaluation of a Mixed Mode ER Engine Mount via Hardware-in-the-Loop Simulation," *Journal of Intelligent Material Systems and Structures*, Vol. 10, pp. 671-677.

[2] Lou, Z., Ervin, R.D., Filisko, F.E., and Winkler, C.B. (1993) "An Electrorheologically Controlled Semi-Active Landing Gear," *SAE Technical Paper Series* 931403.

[3] Lou, Z., Ervin, R. D., Filisko, F.E. (1994) "A Preliminary Parametric Study of Electrorheological Dampers," *ASME, Journal of Fluids Engineering*, Vol. 116, No. 3, pp. 570-576.

[4] Gavin, H.P., Hanson, R.D., Filisko, F.E. (1996) "Electrorheological Dampers, Part I: Analysis and Design," *ASME Journal of Applied Mechanics*, Vol. 63, pp. 669-675.

[5] Gordaninejad, F., Ray, A., and Wang, H. (1997) "Control of Forced Vibration Using Multi-Electrode Electrode-Rheological Fluid Dampers," *ASME Journal of Vibration and Acoustics*, Vol. 119, pp. 527-531.

[6] Sims, N.D., Peel, D.J., Stanway, R., Johnson, A.R., and Bullough, W.A. (2000) "The Electrorheological Long-Stroke Damper: A New Modelling Technique with Experimental Validation," *Journal of Sound and Vibration*, Vol. 229, No. 2, pp. 207-227.

[7] Stanway, R., Sproston, J.L. and El-Wahed, A.K. (1996) "Applications of Electro-Rheological Fluids in Vibration Control: a Survey," *Smart Materials and Structures*, Vol. 5, pp. 464-482.

[8] Stanway, R., Sproston, J.L. and Stevens, N.G. (1987) "Non-Linear Modelling of an Electro-Rheological Vibration Damper," *Journal of Electrostatics*, Vol. 10, pp. 167-184.

[9] Williams, S., Rigby, S.G., Sproston, J.L., and Stanway, R. (1993) "Electrorheological Fluids Applied to an Automotive Engine Mount," *Journal of Non-Newtonian Fluid Mechanics,* Vol. 47, pp. 221-238.

[10] Kamath, G.M., Hurt, M., and Wereley, N.M. (1996) "Analysis and Testing of Bingham Plastic Behavior in Semi-Active Electrorheological Fluid Dampers," *Smart Materials and Structures*, Vol. 5, No. 5, pp. 576-590.

[11] Wereley, N. M. and Pang, L. (1998) "Nondimensional Analysis of Semi-Active Electrorheological and Magnetorheological Dampers Using an Approximate Parallel Plate Model," *Smart Materials and Structures*, Vol. 17, pp. 732-743.

[12] Abramowitz, M. and Stegun, I. A. (1972) *Handbook of Mathematical Functions with Formulas, Graphs, and Mathematical Tables, 9th printing.* New York: Dover.

[13] Wereley, N. M. (2003) "Nondimensional Analysis of Electrorheological and Magnetorheological Dampers Using a Herschel-Bulkley Constitutive Model," *Proceedings of IMECE'03*, Washington, D.C., USA, November 15-21.